Chapter 2
Arthropod Corneal Nanocoatings: Diversity, Mechanisms, and Functions

Mikhail Kryuchkov, Artem Blagodatski, Vsevolod Cherepanov, and Vladimir L. Katanaev

Abstract Corneal surfaces of terrestrial insects and other arthropods are covered with elaborate nanocoatings. Initially described as moth-eye nanostructures – paraboloid nipple-like evaginations regularly assembled on the lenses of some Lepidopterans – they were in recent years discovered to be omnipresent across insect lineages. In addition to the nipple-type morphology, corneal nanocoatings can be built as ridge-, maze-, or dimple-type nanopatterns, with various transitions among these morphologies seen in different species or even within the same specimen. Varying in the height of dozens to hundreds nanometers, and in the diameter being thinner than the wavelength of the visible light, these nanostructures provide the antireflective function to the surfaces they coat. Additional functionalities, such as water-repelling, antifouling, or antibacterial, could also be attributed to them. Turing reaction-diffusion and the block copolymerization mechanisms of molecular self-assembly have been proposed to guide the formation of corneal nanostructures during insect eye development. Both mechanisms envision interactions of two types of molecular agents with different diffusion and/or hydrophobicity properties as the underlying principle of building of the nanostructures. Using model insect organisms, the molecular identities of these agents can be revealed. These studies will

M. Kryuchkov
Department of Pharmacology and Toxicology, University of Lausanne,
Lausanne, Switzerland

A. Blagodatski
School of Biomedicine, Far Eastern Federal University, Vladivostok, Russian Federation

Department of Pharmacology and Toxicology, University of Lausanne,
Lausanne, Switzerland

V. Cherepanov
School of Biomedicine, Far Eastern Federal University, Vladivostok, Russian Federation

V. L. Katanaev (✉)
Department of Pharmacology and Toxicology, University of Lausanne,
Lausanne, Switzerland

School of Biomedicine, Far Eastern Federal University, Vladivostok, Russian Federation
e-mail: vladimir.katanaev@unil.ch

elucidate the mechanism of formation and diversity of the corneal nanostructures in arthropods. Further, they will lay the ground for bioengineering, *in vivo* and *in vitro*, of novel nanocoatings with desired properties.

2.1   Introduction

In order to interact with the environment, animals use a variety of complex micro- or nano-scale interfaces. Well-studied examples of such interfaces are footpads of geckos covered by microscopic hairs providing adhesive force (Autumn et al. 2000) or cicada wings covered with micro-protuberances, which bring about the water-bane effect (Daly 1970; Watson et al. 2017). Arthropods possess such a general multifunctional environment-interacting integument as the chitin-made shell or cuticle, which can additionally contain proteins, lipids, waxes and cement and is secreted through the apical membrane of the underlying cells (Daly 1970).

In addition to the protective function, the cuticle also procures the properties of antireflection, color, mechano- and chemo-sensitivity, anti- or super adhesiveness, and others. To achieve these functions, the cuticle is covered with functionally active bristles, folds and protrusions of micro- and nano-size (Watson et al. 2017). A particular and very interesting case of arthropod functional coverings can be found on the eye lenses, which are most extensively studied in compound eyes of insects. The compound eye consists of tens to hundreds of individual facets or ommatidia, and every ommatidium is formed by pigment, photoreceptor and cone cells, the latter producing the crystalline cone covered by a corneal lens (Katanaev and Kryuchkov 2011). The lens material is secreted by the cone cells, and the surface of the corneae in many insect lineages is covered by nanostructures. They were first discovered by means of scanning electron microscopy (SEM) in 1962 (Bernhard and Miller 1962) in compound eyes of some moths. These nanostructures were described as arrays of nipples varying in height (generally not exceeding 150 nm) and width (of the range of 100–300 nm). While the regularly packed nipple arrays were the main focus of the earlier studies, less ordered protrusions were also seen (Bernhard et al. 1970; Mishra and Meyer-Rochow 2006; Kryuchkov et al. 2011; Blagodatski et al. 2015). The structural-functional relationships of the nipple arrays have been extensively analyzed, and the main function attributed to them was the antireflection (Liu et al. 2010; Gorb and Speck 2017); their other possible roles relate to the anti-wetting and anti-adhesion effects (Liu et al. 2010; Martins et al. 2013).

Initially, the studies of insect corneal nanostructures were mostly limited to Lepidopterans. With the advance of SEM and atomic force microscopy (AFM), insects of different groups were discovered to harbor other types of corneal nano-coatings, such as parallel ridges (found also in spiders), twisted maze-like structures varying in width and height, and the dimpled nano-pattern seen in various insect orders and also in millipedes (Fig. 2.1) (Aghaeipour et al. 2014; Blagodatski et al. 2015; Watson et al. 2017). These diverse arthropod corneal nanostructures represent
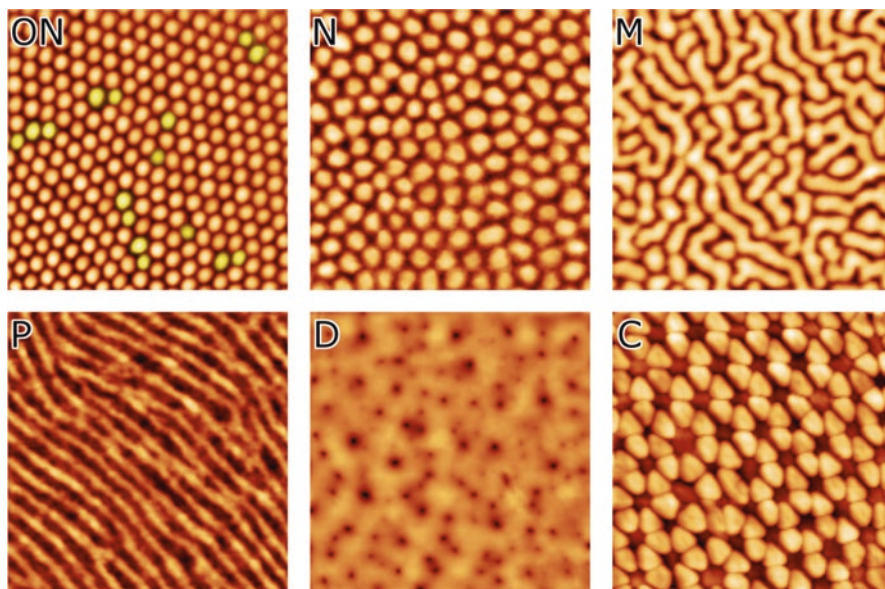
Fig. 2.1 The main types of arthropod corneal nanocoatings. ON – ordered nipples, typical for moths and butterflies. Yellow-labelled nipples indicate coordination defects in the crystal lattice, which form boundaries of highly-ordered domains. N – a non-ordered nipple array. M – a maze-like structure. P – parallel strands. D – a dimpled pattern. C – a special mushroom-shaped hexagonal pattern found on the eyes of *Collembola*. Each square is 3×3 μm

a fascinating object for structural and functional research on organisms' integuments. They are easily accessible for microscopy analysis and can be artificially modified in the genetic model insect *Drosophila melanogaster* (Kryuchkov et al. 2011).

Artificial biomimetic micro- and nano-structured surfaces represent a rapidly developing domain of modern technology (Liu et al. 2010; Gorb and Speck 2017). According to rough estimates, the profit in the global market of materials with nanostructured surfaces will reach approximately 14.2 billion USD by 2022 (Wood 2017). Therefore, the necessity for cheap and simple methods for their production increases yearly. Most methods for creation of nanostructures involve usage of ultraclean rooms, high temperatures, X-ray treatment, and aggressive chemical treatment (Martins et al. 2013; Aghaeipour et al. 2014; Schuster et al. 2015). At the same time, the biological nanostructures of the insects' eyes are formed under mild conditions in the absence of exposure to corrosive chemical compounds. Understanding of the exact features that set the functional properties of the nanostructured eye surfaces of arthropods and of the mechanisms underlying their formation will bring us closer to the possibility of low-cost engineering of artificial nanostructured biomimetic surfaces with desired traits. One famous example is the inspiration of antireflective nanocoatings of photoactive materials in high performance solar cells from the nano-nipple moth-eye nanostructures (Brongersma

et al. 2014). Another – the development of self-cleaning and anti-fouling surfaces for medical applications following natural micro-structured designs (Bixler et al. 2014).

2.2 Functions of Corneal Nanostructures

2.2.1 *Optical Properties of the Arthropod Eye Nanocoatings*

Arthropod integuments in general and the corneal nanocoatings in particular contain chitin, proteins, and lipids (Anderson and Gaimari 2003; Nickerl et al. 2014). These materials are dielectric, meaning that they can be polarized by an applied electric field, cannot conduct electricity, and (importantly for their optic properties) have very low conductivity and polarization losses at optical frequencies – meaning that they are, by default, transparent. Therefore, the following discussion will touch upon the optical properties of dielectric nanostructured materials, while the conductive features of biomimetic nanocoatings will not be covered.

Historically, the first described property of the arthropod corneal nanocoating was the anti-reflectivity (Bernhard et al. 1965; Miller 1979; Blagodatski et al. 2014) increasing the quantity of light transmitted into the eyes and eradicating (to less than 1%) the amount of reflected light – the latter also contributing to the decreased visibility of nocturnal insects to predators (Miller 1979; Stavenga et al. 2006).

Due to a large difference between the refractive index of air and that of the lens of the eye – 1 *vs*. 1.5–1.8 (Varela and Wiitanen 1970; Meyer-Rochow 1978; Toh and Okamura 2007) – part of the incoming light does not reach the photoreceptor cells and is instead reflected from the lens. The reflected part can be calculated according to the Fresnel equation and equals 4–8% of the incident light. This problem can be compensated at the level of the size of individual ommatidia or the compound eye as a whole. The former solution relates to enlargement of the lens area or thickness. The latter – to the overall increase in the eye size through multiplying the number of ommatidia. Both solutions are limited by the maximal possible size of an ommatidium and of the insect itself.

As a direct approach to the problem, the amount of light transmitted into the eye can be increased through minimizing the amount of the reflected light, by means of the following alternative mechanisms. The first relies on a film positioned between the lens and the air, with the refractive index intermediate of the two media. If the film thickness is an odd multiple of $\lambda/4$, where λ is the light wavelength, then the beam reflected from the second interface (film and lens), will be out of phase with beam reflected from the first interface (air and film). These two beams will interfere and cancel each other, thereby decreasing the energy of the reflected light (Fig. 2.2A). Although used in many technological applications, this approach is limited to a particular angle and wavelength of the incoming light (Raut et al. 2011), which becomes problematic for eyes of the superposition type (Stavenga 2006) or with small, strongly convex ommatidia (Meyer-Rochow and Stringer 1993). The second
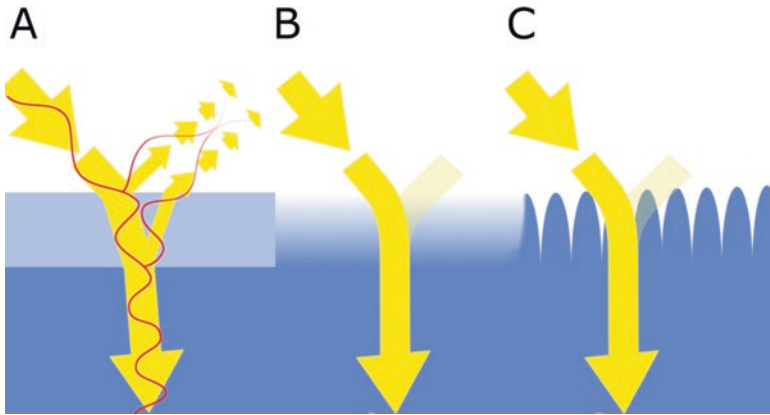
Fig. 2.2 Different designs of antireflective coatings. For a single-layer film (**A**), the two reflected waves may interfere cancelling each other. This coating functions for selected wavelengths and incident angles. An ideal antireflective coating (**B**) gradually approximates the refractive index of the incoming medium to that of the receiving medium. If the surface is coated with structures with dimensions smaller than the light wavelength (**C**), light interacts with the surface as if it has such a gradient of refractive indices

approach is an approximation to the ideal Rayleigh's film and relies on the fact that the sum of reflections from two interfaces is less than reflection from one interface, provided that the refractive index of the film is intermediate between those of the surrounding media. With this approach, multiple film layers gradually decreasing refractive indices from that of air to that of the lens should be coated (Fig. 2.2B) (Raut et al. 2011).

The third alternative produces largely an angle-independent effect and relies on the coating with structures, which cannot be resolved by the incident light, i.e. whose diameter is smaller than the wavelength of incoming light for perpendicular incidence and smaller than half-wavelength for oblique incidence. Under these conditions, the effective refractive index at any given depth of the coating is the sum of refractive indices of the coating materials multiplied by their proportions at that depth. That is, if at a given depth of the coating, half of the cross-section is filled with the lens material and the other half – with air (Fig. 2.2C), the effective refractive index at this level will be exactly between that of the air and that of the lens material. Quanta of light go through such nanostructured coating like through the medium with a smooth gradient of refractive index (Wilson and Hutley 1982; Deinega et al. 2011; Raut et al. 2011) (Fig. 2.2C). The antireflective function depends on the shape and location of nanostructures, and can be accurately determined by numerical solution of Maxwell's equations. One of the commonly used methods to obtain an approximate solution to these equations is FDTD (finite-difference time domain) (Deinega et al. 2011). Simulations based on these approximations correlate well with the experimental data (Daglar et al. 2013; Aghaeipour et al. 2014; Yu et al. 2015; Xin et al. 2016).

An increase in the diameter of nanostructures (Aghaeipour et al. 2014; Yu et al. 2015) or of the distance among them (Son et al. 2011) increases the wavelength of light with the maximal reduction in reflectance. This feature provides a way to fine-tune light transmission to the wavelengths needed for a particular insect's life style. Accordingly, different insects possess corneal nanostructures with different widths. For example, maze-like structures on the surface of ladybirds' eyes are 100–200 nm broad (sometimes going down to 50 nm), while similar structures in a Staphylinidae beetle have an atypical width of 400–500 nm (Blagodatski et al. 2015).

Another important dimensional characteristic of the nanostructures is their height. Several theoretical and experimental studies on ordered structures have demonstrated that the higher the structures are, the less light they reflect (Stavenga et al. 2006; Deinega et al. 2011; Raut et al. 2011). Using the predatory Neuropteran *Libelloides macaronius* with the eyes split into dorso-frontal and ventro-lateral halves, we have directly shown that a mere increase in the nanostructures' height from 8 to 32 nm decreases by 20–40% (depending on the wavelength) the amount of reflected light in the dorso-frontal half relative to the ventro-lateral one (Kryuchkov et al. 2017b). The trade-off here is that higher nanostructures are more susceptible to injury with subsequent loss of functionality. The evolutionary pressure in this case provides conflicting demands: to maximize the efficiency of the nanostructures on one hand, and to minimize the risk of losing them by harsh interactions with the environment, on the other. This conflict is illustrated by the fact that flying insects such as butterflies can afford higher nanopillars than the crawlers who are confronted with a bigger risk of collision with the substrate and resulting damage to the eye surfaces. The highest known protrusions are the highly-ordered nipples from *Euxanthe wakefieldii* butterflies of the Nymphalidae family with a height of 230 nm (Stavenga et al. 2006). At the same time, the minimum height of nanostructures is around 10 nm (10 nm for Lepismatidae, 5–15 nm for Platycnemedidae, 8–15 nm for Scutelleridae) (Blagodatski et al. 2015).

The shape of corneal nanostructures is another characteristic important for their function. It can be convex or concave, cylindrical or conical, and each may have its own advantages depending on other conditions (height, density, and ordering). Theoretical considerations indicate that the refractive index gradient is the smoothest for linear cones, although these calculations are valid only for the structures taller than 250 nm (Ji et al. 2012; Han and Zhao 2014; Siddique et al. 2015). Cone-shaped nanostructures have been found as the most effective anti-reflectors also in the case of the low angle of the incident light (Stavenga et al. 2006; Ji et al. 2012; Leem et al. 2012).

Insects' corneal protrusions do not exceed 250 nm due to mechanical instability of higher structures. As opposed to the cone shapes, nanostructures of the convex form were shown to be effective at the height < 100 nm for the visible and UV light (Stavenga et al. 2006; Ji et al. 2012; Leem et al. 2012; Daglar et al. 2013). Among different possible convex structures, bullet-like bi-paraboloid shapes have been described to grant maximal antireflection efficiency at the wavelengths of 300–800 nm (Leem et al. 2012). According to the existing data, most insects indeed possess nanostructures of the convex shape, with a slight bullet-shape outline (Stavenga et al. 2006).
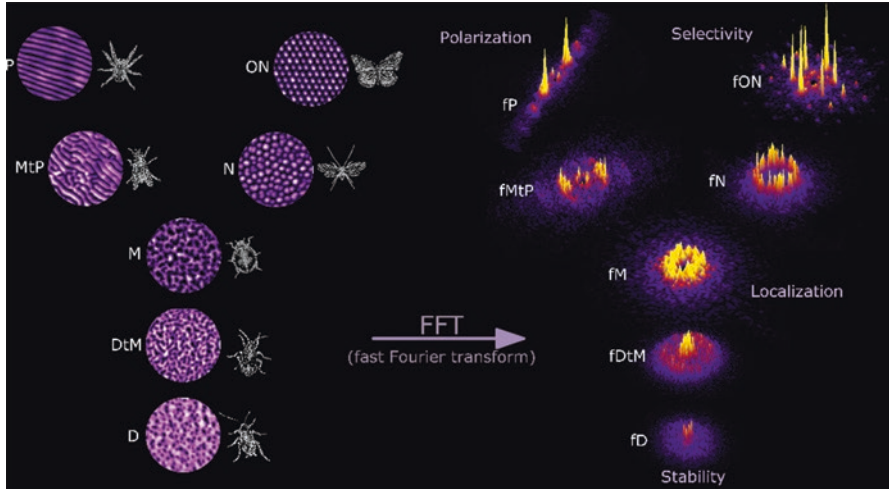
Fig. 2.3 Fourier analysis of different corneal nanostructures in relation to their possible properties. D: dimpled pattern from Blattidea, DtM: dimple-to-maze transition from Hemiptera, M: maze-type from Coleoptera, N: nipple-like structures from Psocoptera, ON: highly ordered nipples from Lepidoptera, MtP: maze to parallel strands transition from Diptera, P: parallel strands from a true spider. The prefix "f" denotes 2D Fourier transform of the corresponding structure. In the order from bottom to top, physical stability decreases, while selectivity for the light wavelengths increases. Non-ordered structures can localize the beam of light. Parallel strands can polarize the incident light and transfer it in the unidimensional manner with a minimal loss of energy

Another characteristic affecting the anti-reflectivity of nanostructured surfaces is the degree of order in the packing of the nanostructures, which is linked to the uniformity of their shape and dimensions, as well as with the packing density. A common way to analyze the degree of order and the packing density is FFT (fast Fourier transform, referred to as 'Fourier transform' throughout the text) (Wiersma 2013). Existence, position, and sharpness of reflexes in Fourier transforms speak about the degree of crystallinity in the packing. For example, clear reflexes in the corners of the hexagon show that the structures are hexagonally packed, representing high order (ON and fON structures of Fig. 2.3). In contrast, fusing of reflexes into concentric circles indicates lack of order in the packing yet uniformity of the dimensions of the densely packed individual nanostructures (N and fN structures of Fig. 2.3) (Kryuchkov et al. 2011; Wiersma 2013). The level of disorder is reflected in the Fourier transforms by the form and size of the area with prominent peaks (Martins et al. 2013). Correspondingly, fusion of protrusions into mazes (M, fM on Fig. 2.3) and the further merge of maze-like forms into dimpled patterns (DtM and D, fDtM and fD on Fig. 2.3) are reflected in the Fourier transforms by merging of the concentric circles into a solid disk with subsequent reduction of its size. It is thus evident that the packing order in insect nanocoatings decreases in the direction from highly ordered nipple arrays to the non-ordered ones, then to maze-like structures

and further to dimpled patterns (Martins et al. 2013; van Lare and Polman 2015) (Fig. 2.3).

Regarding the highly ordered *vs.* disordered nipple arrays, numerous studies have shown that higher degrees of order increase the amount of reflected light in comparison to non-ordered protrusions, but enhance the wavelength's selectivity (Fig. 2.3) of the allowed transmitted light. In contrast, disordered nanostructures allow the transmission of light of a broader wavelength range, leading to a bigger quantity of the total transmitted light (Du et al. 2011; Oskooi et al. 2012; Zhou et al. 2015).

Further, higher order increases the haze intensity, whereas disordered or quasi-random structures result in reduced light scattering (Zhou et al. 2015). Another potential problem associated with the highly ordered arrays of nanostructures is the strong intensity of the −1 diffraction order appearing at high angles of incidence. In other words, the highly ordered arrays, while providing a general anti-reflectivity, suffer from the intense glare emanating from the surface if viewed at a particular high angle – which would be problematic in terms of the attempts of the insect to camouflage itself from prey or predators. In contrast, if the surface is covered by 2D–crystalline patches of different orientations, the glare is dramatically reduced (Stavroulakis et al. 2013). It is thus not surprising that in the insect corneal nanocoatings built by highly ordered nipple arrays, the high degree of order exists within clusters separated by more disordered borders (Fig. 2.1 ON). In addition to the potential need for such organization for the antiglare function, this effect is also an unavoidable consequence of the curvature of the lens, as in any convex polyhedron decorated with hexagons, there have to be pentagons as defects, like in a soccer ball (Sergeev et al. 2015; Lee et al. 2016).

The maze-type nanocoating produce the blurred circle-like form of the peaks of reflexes in the Fourier transform (Fig. 2.3) This type is intermediate between fully disordered and (quasi-)ordered structures and has been called a quasi-random type of organization; it may be effective as a broad-band antireflective surface (Martins et al. 2013).

The most disorganized (but still not fully random) yet mechanically stable structures are the dimpled patterns or nano-holes (Fig. 2.3). The dimple parameters (diameter and depth) influence the light transmission (Son et al. 2011), but other factors are also important. Indeed, corneae of the domesticated silkmoth reflect up to 40% more light than the corneae of its wild ancestor *Bombyx mandarina*, yet the average dimensions of nanostructures in these species remain approximately the same. It is the type of nanostructures which changes from fully random sponge-like coating in *Bombyx mori* to the quasi-random nano-holes of *Bombyx mandarina* (Kryuchkov et al. 2017a), agreeing with some experimental findings in artificial surfaces (Son et al. 2011; Lin et al. 2013; Pratesi et al. 2013).

Upon increasing in the ordering of maze-type structures, another type of highly packed structures emerges: parallel rows (Fig. 2.1 P, MtP and P on Fig. 2.3). The parallel strands, unlike nipples, can maintain their crystallinity throughout the entire surface of the lens and thus achieve a higher degree of order. These structures may mediate some unique optical functions. Subwavelength rows are anisotropic formations, which could produce different phase shifts for the transverse electric and

transverse magnetic polarized incident light, allowing functioning of these formations as polarizers (Fig. 2.3). A similar function was previously attributed to parallel strands, formed by filaments covering bracts of edelweiss flowers (Vigneron et al. 2005). Such all-dielectric nanostructures would function in the way different from the metal polarizers and described by the elementary diffraction potential theory and approximations of the effective-medium theory (Lin et al. 2014; Yoon et al. 2015).

Corneal parallel strands can be organized in two different ways (Blagodatski et al. 2015). The first patterns the entire corneal surface by parallel rows and can be found in some spiders and may function as a polarizer of the incident light. The second employs radiation of the strands from the center of an ommatidium to its periphery; the center in this case is often covered by nipple-like nanostructures (Meyer-Rochow and Stringer 1993; Blagodatski et al. 2015). This way of patterning can be found in many Dipterans (Blagodatski et al. 2015), including an extinct dolichopodid fly from Eocene amber (Tanaka et al. 2009). Such organization may also result in light polarization. It could also be beneficial to boost the antireflection functionality for insects with small ommatidia with the resulting strongly convex surface, such as those of *Leucoptera coffeela* (Meyer-Rochow and Stringer 1993). In such ommatidial shapes, the vertical incident beam is perpendicular to the surface only in the center of the lens – which is covered with nano-nipples. Towards the edges of the lens, nippled structures will reduce their functionality, as they light beam entering a nipple will transverse it and enter the air-filled concentric inter-nipple space, before entering another nipple and finally the lens. Substitution of the nipples with radial parallel ridges with similar widths and heights brings back the functionality.

2.2.2 Anti-Wetting, Self-Cleaning and Antimicrobial Properties of Arthropod Corneal Nanocoatings

Another important feature of the nanocoatings is that they may change the wettability of the material of which they are built. There are no less than six different theoretical models describing interactions among rough materials, gases, and liquids; the two extremes among these models are the Wenzel and the Cassie-Baxter models. The Wenzel model presumes complete wetting of the entire surface of the material, whereas the Cassie-Baxter model suggests that gas is trapped in all the cavities formed by the roughness of the solid material. Experimental data show that the real solid-liquid-gas interactions represent different intermediates between these two models and depend on the morphology of the structures (Sun et al. 2005).

There are two well-known natural examples of the interactions of structured surfaces and liquids. These are the "Petal effect" and the "Lotus effect". The red rose petals are coated by micropapillae harboring nanoprotrusions. However, between the papillae the surface is smooth, which increases the adhesion of the liquid. This structuring leads to a decrease in the spreading of the droplet over the surface (a super-hydrophobic surface with contact angle >150°), but at the same time it keeps the

drop from rolling-off. The lotus leaf coating layer has a rough surface and a low contact angle hysteresis, which means the water droplet is not able to wet the microstructure as in the Cassie-Baxter model and the liquid can roll-off easily (a super-repelling surface with the contact angle >150° and roll-off angle <10°). This effect allows not only avoiding retention of liquids on the surface, but also makes it easy to clean the surface with water (Sun et al. 2005, 2012; Feng et al. 2008; Liu and Kim 2014).

In the work on mutant *Drosophila*, it has been proposed that the change in adhesion force and hence the surface energy depends on the chemical nature of the nanocoating (Lavanya Devi et al. 2016). However, as the exact composition of corneal nanostructures remains unknown, we will focus only on the adhesion properties resulting from the morphology of the eye surface.

Super-hydrophobicity of an insect's eye has been directly proven in experiments with eyes of mosquitoes, monitoring failure of nucleation of tiny fog drops on their surface (Gao et al. 2007). In our previous work, we have illustrated that the maze-type nanocoating of the corneal lens of Gyrinidae whirligig beetles does not provide any additional hydrophobicity in comparison with a smooth surface. Analysis of the contact angles of the droplets of water placed on these surfaces produced almost identical results, less than 90° (Blagodatski et al. 2014) (Fig. 2.4). In (Peisker and Gorb 2010) it was shown that hydrophobic properties of corneal nanostructures could be calculated by using the JKR (Johnson-Kendall-Roberts) model, and these data fit very well with experimental results demonstrating that hydrophobicity is positively correlated with the height and density of the convex-formed protrusions (Sun et al. 2012) (Fig. 2.4).

Cuticle of small Collembola hexapods, including their corneae, is covered with unique mushroom-shaped nanostructures (Figs. 2.1C and 2.4) (Nickerl et al. 2014). Curiously, size of these nanostructures varies widely on the body surface, but is minimal on the eye surfaces, likely accommodating the antireflective function as the

Fig. 2.4 Anti-wetting properties of different types of insect corneal nanocoatings. First column – 3D images of corneal nanostructures (each square is $2 \times 2 \, \mu m$). Second column – schematic interactions of $1 \, \mu m$ cross-sections of the nanocoatings with water (blue). Air bubbles (white) are trapped in the 'pockets' of the nanostructures of *Clossiana* and Collembola, mediating the effect of super-hydrophobicity
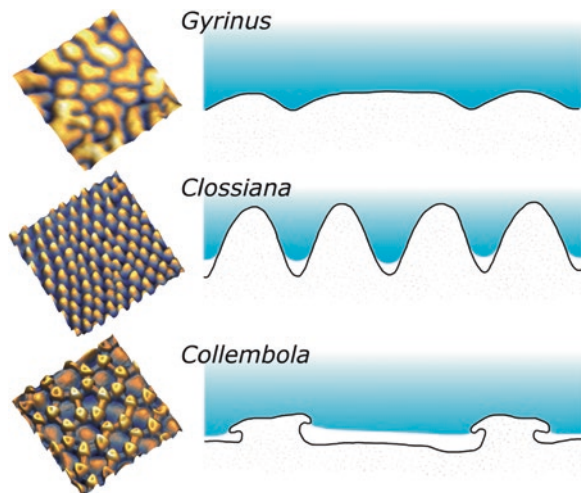
other types of corneal nanocoatings described above. However, the main function of these Collembola nanostructures is hydrophobicity: trapping air bubbles in the 'pockets' at their basis, they prevent effective liquid-surface interactions (Helbig et al. 2011; Hensel et al. 2016) (Fig. 2.4). In fact, these structures are not only super-hydrophobic, but display omniphobicity, as the body of Collembola cannot become wet neither in water nor in oil or alcohol (Helbig et al. 2011; Hensel et al. 2016). Curiously, these mushroom shaped structures are remarkably similar to synthetic structures fabricated in SiO_2 by Liu and Kim (2014) that super-repel all liquids, including perfluorohexane, which has never been observed to form the spherical drop, and *a fortiori* to roll off from any surface.

In continuation of this topic, it could be argued that adhesiveness to nanostructured surfaces is reduced not only for liquids but also for biological objects like bacteria. Indeed, such surfaces play a strong antibacterial and antifungal role, and allow microbes neither to attach to nor to grow on them (Helbig et al. 2011). Such observations have been made e.g. with the cicada wing nanocoatings and with artificial materials bioinspired by the cicada wings (Green et al. 2012). Moreover, when exposed to water vapor, cicada wing surfaces can display self-cleaning from contaminating particles through the self-propelled jumping mechanism of the liquid condensate (Wisdom et al. 2013). The same effect can be expected (but has not yet been experimentally observed) for the very similar eye nanocoatings, such as the butterflies' highly-ordered corneal protrusions (e.g. *Clossiana* genus, Fig. 2.4).

The antibacterial function can be fulfilled not only due to the anti-adhesive properties, but also through the small curvature radius of the nanostructures' peaks. This feature causes stretching of the bacterial cell wall on the nanostructures and results in mechanical laceration of bacteria and cell death (Ivanova et al. 2012; Pogodin et al. 2013; Xue et al. 2015).

In addition to the effects of the lotus leaf and rose petal, there also exists the so-called rice leaf effect (also known as the butterfly wing effect). Both surfaces are special by the anisotropy of the coating structures, i.e. the presence of parallel formation differently affecting the tendency of fluids to flow in transverse *vs*. longitudinal directions (Sun et al. 2005; Hancock et al. 2012; Bixler and Bhushan 2014). The resembling corneal nanocoatings, such as the radiating ridges in some Dipterans (Fig. 2.1 P and P on Fig. 2.3), could also be expected to direct the removal of contaminants towards the edges of the ommatidium.

2.3 Hypotheses of Formation of Corneal Nanostructures

2.3.1 Physical, Chemical and Biological Mechanisms of Formation of Corneal Nanostructures

Initially, as the corneal nanostructures had been known only in the form of ordered Lepidopteran nipple arrays, with other types understudied or regarded as insignificant irregularities (Bernhard et al. 1970), it was postulated that the nipple-like

protrusions are formed in the developing eye by secretion from the regularly spaced microvilli of the cone cells (Gemne 1966, 1971; Bernhard et al. 1970; Fröhlich 2001). Later studies revealing existence of alternative nanostructural patterns have set this hypothesis under question. Indeed, the microvillied cell surface somewhat resembles the nippled corneal pattern but, given the current diversity of the arthropod eye nanostructures and a variety of transitions among them, sometimes even within the same lens (Blagodatski et al. 2015), this hypothesis is not satisfactory any more. Instead, several other concepts, partly complementing each other, have been proposed, suggesting that specific mechanisms of patterning at the nanoscale are involved. These mechanisms assume formation of nanopatterns through a series of physical and chemical interactions and are discussed in the following subsections.

2.3.1.1   The Reaction-Diffusion Model

It has been noticed that the diversity of corneal nanostructures in arthropods is remarkably similar to the set of the patterns described by Alan Turing in his famous reaction-diffusion system (Turing 1952; Blagodatski et al. 2015). This system of differential equations shows how two reacting morphogens – a slowly diffusing activator and a fast diffusing inhibitor – can provide a broad variety of biological, chemical, and physical patterns, previously demonstrated to work at the macro- and micro-scale (Sick et al. 2006; Nakamasu et al. 2009; Raspopovic et al. 2014). The arthropod corneal nanopatterns are different from these prior examples in the sense that they represent not just one of the many possible forms described by the reaction-diffusion model, but a complete set of all possible variants including the intermediate forms. Such complete coverage of the modelled patterns with those found in nature provides a strong argument in favor of the hypothesis that the corneal nanopatterns are indeed a product of the Turing reaction-diffusion mechanism. The reaction-diffusion model allows producing patterns only in a certain range of parameters (activation, inhibition and diffusion constants); outside of the permitted parameter space, no stable patterns can appear. Mathematical Turing modeling of corneal nanopattern formation has shown that the nanoscale patterns are expected to form under conditions where diffusion properties are reduced (in comparison to the liquid phase), corresponding to the reaction-diffusion system acting in colloidal or liquid crystal-type environment, similar to that of the developing eye lens. Importantly, a set of patterns has been modeled with dimensions identical to those of the experimentally described insect corneal nanocoatings, and all the modeling parameters thereof were found inhabiting the parameter space predefined for the Turing patterns, thus also speaking in favor of the hypothesis (Blagodatski et al. 2015). Remarkably, while different combinations of the reaction-diffusion parameters can produce different nanopatterns in the model, simulations reveal that three of the four main corneal pattern types found in arthropods belong to defined regions within the parameter space and transform one to another in the following way: dimples ↔ mazes ↔ nipples. The dimpled pattern appears to be the most primitive in this system, since it requires minimal values of the diffusion parameters. It might

have emerged first during arthropod evolution when these parameters just exceeded the threshold values, allowing the generation of the Turing-type structures (Miura and Maini 2004; Kondo and Miura 2010; Blagodatski et al. 2015). The primordiality of the dimpled pattern is also indirectly suggested by the fact that it is typical for centipedes (Blagodatski et al. 2015), which are presumably the closest taxon to the ancestral primitive arthropods (Chipman et al. 2014). The structures with the highest degree of order, such as the hexagonally packed nipple arrays or parallel strands, evolve in this model from their predecessors (irregular nipples and maze-like structures, respectively, Fig. 2.3) when the diffusion coefficient of the activator reaches its maximally allowed levels within the parameter space. On the other hand, the maximal possible values of the inhibitor diffusion coefficient bring the system to increase in the width of the nanostructures (nipples or ridges, respectively) (Blagodatski et al. 2015).

2.3.1.2   Formation of Order in the Nipple Arrays

Among the variety of corneal nanostructures, the "classical" hexagonally packed nipple arrays have received the most interest so far. They have been analyzed from various points of view, including regarding them as crystal lattices and studying them by AFM, SEM and mathematical modeling. These nanopatterns have also been the focus of analysis addressing the origin of order in nanostructures. Thus, nippled nanocoatings of representatives of six different insect orders (Diptera, Lepidoptera, Psocoptera, Hemiptera, Trichoptera and Thysanura) were studied with a special algorithm, permitting simultaneous assessment of geometric characteristics of the nanostructures (such as height, width, inter-nipple distance) in relation to the regularity of the nipple packing (Sergeev et al. 2015). The regularity was determined by mutual orientation of the neighboring nipples and, by analogy with condensed matter science, nipples that did not possess exactly six neighbors were characterized as defects, which are made either by vacancies in the densely packed arrays or/and by non-equal sizes and shapes of nipples. Defects of the nipple "crystal lattice" were predominantly detected between hexagonally-packed ordered domains, which varied in diameter from 2 to 12 μm in different insects (Sergeev et al. 2015). These defects effectively form the domain boundaries (Fig. 2.1 ON). Degree of order in the nipple arrays was characterized by the hexagonal packing coefficient (HPC) – the relative number of grains with a coordination number (the number of nearest neighbors) equal to 6: the greater the HPC, the higher is the packing order. The HPC values revealed a positive correlation with the nipple packing density and the nipple height, negative correlation with the nipple diameter and the inter-nipple distance, and no correlation of HPC with the lens size or the nipple volume. This led to conclude that patterning mechanisms such as described by Turing probably coexist with the packing density forcing appearance of order in the biological nanostructures. Dense packing leads to formation of more ordered arrays of taller and thinner nipples with smaller inter-nipple distances. External patterning mechanisms may be at play to provide the initial positioning of the nanostructures and/or to elicit the

interactions among the building blocks, thus opening a possibility for the dense packing to serve as the driving force responsible for the order formation. Analysis of the degree of order and of the order generation mechanisms in other types of nanopatterns such as mazes or parallel ridges is subject of further investigation.

As an extension and complementation to the reaction-diffusion mechanism, a nucleation and growth mechanism similar to that acting during formation of crystals has been proposed (Lee et al. 2016). Similarly to the previous study (Sergeev et al. 2015), corneal nipple arrays of the butterfly *Nymphalis antiopa* were regarded as a crystal lattice and analyzed by SEM at the nanoscale to study the crystal and defect structures, and at the mesoscale to estimate the crystal domain sizes as well as the orientations between the domains over the entire ommatidium. The results obtained were in general consistent with the previous study. At the nanoscale, vacancies and fusion defects were found at a low frequency. The 5–7 coordination defect predominated and was found almost exclusively at boundaries between adjacent domains with the perfect hexagonal structure, in a manner similar to grain boundaries in 2D hexagonal structures (Lee and Erb 2013, 2015). At the mesoscale, rows of 5–7 coordination defects were found to form an interconnected network of domain boundaries, subdividing the entire ommatidium into numerous domains (about 120 per facet), each containing nipples in the perfect hexagonal arrangement (Lee et al. 2016). Very little order was found at the ommatidial boundaries and triple junctions; no indications of crystals or crystal orientations extending from one ommatidium to a neighboring one were seen. Generation of multiple domains within a single ommatidium can be explained by the Turing model, when a cascade of independent pattern formations is initiated by local fluctuations of the activator/inhibitor concentrations, each formation responsible for a discrete domain. Mathematical simulations of the nipple "nucleations", which could potentially be triggered in numerous locations, filling the lens surface with multiple sets of ordered hexagonal arrays, have been performed. It was found that the Turing modeling allows covering areas large enough to fill the entire ommatidium, without requiring existence of pre-patterning cone cell microvilli (Lee et al. 2016). However, microvilli might still contribute to the pattern formation e.g. as initiators of nipple "nucleation" or by providing means to control the activator/inhibitor concentrations during eye development.

2.3.1.3   The Block Copolymer Model of Nanostructure Formation

Being an impressive explanation of the general principle of nanopattern formation, the reaction-diffusion model currently lacks the specifics on the exact chemical identities of the molecules interacting during developing of the nanostructures. A potent example of *in vitro* self-assembly of nanoscale patterns resembling that of arthropod corneae (Figs. 2.1 and 2.5), which may give a clue to a possible chemical nature of their mechanism of formation, is provided by the block copolymer (BCP) systems. Block copolymers are made of blocks of different polymerized monomers (styrene and methylmethacrylate being classical examples). Due to different hydrophilicity/hydrophobicity of the blocks, block copolymers are capable of microphase
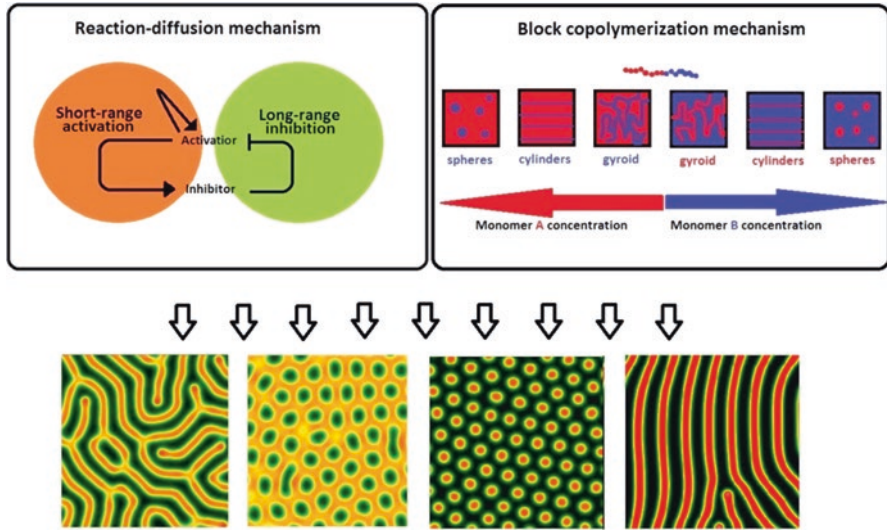
Fig. 2.5 The reaction-diffusion mechanisms (above left) driven by short-ranged and long-ranged interactions of a slowly diffusing activator and a fast diffusing inhibitor, as well as block copolymerization (above right) driven by physico-chemical interactions and concentration ratios of two polymerizing monomers with different physical properties, give rise to similar patterns defined as spheres, cylinders and gyroids (above right) in case of block copolymerization or as mazes, dimples, nipples, or ridges in case of arthropod corneal nanostructures (below)

separation – a process similar to phase separation of oil and water. Because the blocks are covalently bound to each other, they cannot demix macroscopically as two liquids would, separating in microscale and forming nanometer-sized structures instead (Hamley 1998; Hamley et al. 2004). Self-assembly in BCP systems is driven via a thermodynamic process where chemical dis-affinity between the blocks separating them is balanced by a restorative force derived from the chemical bonds between the blocks (Farrell et al. 2009). Block copolymerization can serve as a tool to engineer nanostructured thin films, where patterns similar to nipples, dimples, ridges and mazes can be found, albeit markedly smaller in dimensions than those found on arthropod eyes: their usual thickness is about 5–50 nm (Wu et al. 2005). Interestingly, artificial design of nanopatterns from block copolymers often requires a careful chemical and topographical pre-patterning of the surface upon which they are formed (Farrell et al. 2009). In the case of chemical pre-patterning, the substrate surface is treated with a compound that selectively chemically interacts with one block of the copolymer, so that the micro-phase separated structure tends to align to the pre-pattern (Chen and Chakrabarti 1998). Surface topography plays a role in formation of the nanostructures along with chemical properties of the substrate. The graphoepitaxy (topographical alignment), first described in Fasolka et al. (1997), is an example of topographical pre-patterning, where a single relatively large substrate feature such as a channel can be used to direct the BCP nanopattern with precise alignment into almost single crystal-like periodicity within such a channel (Farrell

et al. 2009). Graphoepitaxical photolitography-based pre-patterning has been used to influence the form of nanopatterns created by block copolymerisation, resulting in formation of parallel nano-strands on a pre-patterned surface by a polystyrene-block-polymethylmethacrylate copolymer, which otherwise formed maze-like structures on untreated or undertreated surfaces (Kim et al. 2003). In another example, pre-patterned grooves were used to create cylinder arrays resembling those of regular nipples using the same copolymer (Xiao et al. 2005). Thus, not only the chemical nature of molecules forming the nanopatterns, but also physical or chemical pretreatment of the environment where they are formed affects the nanostructural features. This can bring to a reconsideration of the potential role of the cone cell microvilli in development of the corneal nanostructures. Indeed, the microvilli might not be directly used for secretion of nipple arrays or other nanostructures but may instead serve, either through forming the basement for the nanostructures or through production of some metabolites, as a chemical or topographical pre-patterning tool for the nanopatterns. Another hint can be that the form of the ommatidia itself serves as a kind of a template directing the nanostructural development. The two mechanisms – the Turing reaction-diffusion system and the BCP system – can generate very similar patterns (Fig. 2.5) and involve interactions of at least two chemical entities with different properties. Identification of these entities and recapitulation of the patterns through their admixtures in controlled experiments are required in order to identify the exact mechanism behind the corneal nanostructures.

2.3.1.4 The Genetics of the Nanostructure Formation

In this regard, molecules regulating genesis of the biological nanostructures are of a special interest and remain largely unrevealed. A study on *Drosophila melanogaster* corneal nipples has been performed, not only describing their physical parameters and regularity, but also addressing the question of signaling pathways potentially involved in the development of the nipple arrays (Kryuchkov et al. 2011). Being a thoroughly studied model animal, *Drosophila* allows numerous genetic manipulations with subsequent investigation of the resultant mutant phenotypes (Katanaev and Kryuchkov 2011). We tested the potential role of one of the most important developmental signaling pathways, namely the Wg-Frizzled pathway, in formation of the corneal nanostructures. One of the very first mutants discovered by the 'father' of *Drosophila* genetics Thomas Morgan had been named *Glazed* due to the glossy eye appearance and was decades later revealed to be caused by overexpression of the Wg morphogen, overactivating the Wg-Frizzled signaling pathway (Bhanot et al. 1996). AFM analysis of the nipple arrays of a Wg-overexpressing *Drosophila* line with the glazed eye phenotype demonstrated a drastic loss of nipples, while the remaining degenerated nanostructures were randomly spaced in ommatidia with large gap areas (Kryuchkov et al. 2011). Thus, the glossy appearance of *Drosophila* eyes correlates with the loss of corneal nanostructures. These findings further suggest that development of the corneal nanostructures is influenced (directly or indirectly) by the Wg signaling.

Another application of *Drosophila* as a model organism to study formation of the nanostructures involved an RNAi screen, where a series of genes responsible for cuticle formation and cell polarity were systematically knocked down by RNAi expression or analyzed using the existing mutant collections, in a search for genes affecting the phenotype of corneal nanostructures (Minami et al. 2016). Interestingly, some of the identified glossy eye mutants demonstrate a nipple-to-maze transition (*gl* mutant) and even a maze-like phenotype (*spa* mutant), while other mutations have shown a complete vanishing and degradation of nipples (mutants *lz* and *Glazed*, again). RNAi silencing of some genes also led to partial nipple-to-maze merging (*Cpr49Ah*, *Act5C*) and partial nipple enlargement (*Cpr23B*, *Syx1A*, *Sec61ß*). This study is a proof-of-concept of the possibility to alter the nanostructure type in a model animal using genetic manipulations. However, it would be premature to suspect that the genes identified are the ones directly responsible for e.g. the nipple-maze transition, as these mutant flies demonstrated not merely alterations at the level of the nanostructures but also a drastic disorder at the macro- and micro-levels ("rough eye" phenotypes, merging and degradation of ommatidia, eye size decrease, *etc*.). Thus, the observed nanostructural defects are likely due to indirect effects caused by general disturbances of the eye development which occur frequently during genetic studies on *Drosophila* eye (Katanaev and Kryuchkov 2011).

2.3.2 *Ontogenesis of the Corneal Nanostructures*

Most EM and AFM studies of corneal nanostructures have been performed on corneal samples of adult insects or other arthropods. Presently, surprisingly little is known about larval or pupal formation of the eye nanostructures, although their generation takes place at these earlier development stages.

Early data on pupal development of corneal nanostructures were produced from EM-derived pictures of 1960s–1970s, when the theory of nanostructure formation via microvilli secretion dominated (Gemne 1966, 1971). Extensive EM analysis of the nipple development over an 8-day pupation period of the moth *Manduca sexta* concluded that the nipple arrays are an integral part of the lens surface (Gemne 1971). According to this study, nipple formation begins about 5 days after pupation with the development of initial patches on the epicorneal lamina on top of underlying microvilli. This is followed by formation of the nipple anlage, first as low cupoles, then as higher cupoles after 6.5–7 days. After 7.5–8 days, the high cupoles become filled with the corneal substance through the microvilli and consolidate, forming the final nipple structure. The arrangement of microvilli tips in the cone cells was believed to be organized in the hexagonal packing manner, explaining the observed arrangement of the nipples in hexagonal domains. Defects in the nipple arrangement showing deviation from the perfect hexagonal packing were explained by the convex shape of the lens. Currently, we know that these defects are distributed in a specific manner, lying predominantly on the nipple domain boundaries, as discussed above (Sergeev et al. 2015; Lee et al. 2016). Interestingly, the detailed EM study revealed

that corneal nipples emerge in the very beginning of the lens formation, and the chitinous layer seems to be secreted later, underlying the nanostructures. Thus the chitin itself is unlikely to take part in the assembly of the nanocoatings but merely serves as one of the building materials for the lens itself (Gemne 1971).

The main challenge for the microvilli model is that it lacks explanation for formation of the patterns other than the nipple arrays. In the 1970s, the non-nippled nanostructures were regarded rather as degenerate or underdeveloped structures, whose appearance was linked with defects in the microvilli-lamina evagination bridges on the epicorneal lamina (Bernhard et al. 1970; Gemne 1971). Even if we apply the microvilli theory exclusively to the nipple arrays, it is still hard to explain by its means the formation of boundaries of hexagonally-packed ordered domains with very specific configurations – formed by rows of coordination defects as described in (Sergeev et al. 2015; Lee et al. 2016). The model requires that the initial arrangement of microvilli serves as an exact template for the specific nipple arrangements before the nipples are actually formed. However, this is not the case, since the one-to-one correspondence between the positions of microvilli and the initial patch locations or the final nipple positions is not apparent from the presented electron micrographs (Gemne 1971).

A detailed SEM study was performed on the pupal eye of a developing *Drosophila* (Fröhlich 2001), with a description of corneal nipple formation in parallel with secretion of the lens cuticle at later stages of pupation (42–46 h). Interestingly, the author found that the nipple arrays arise almost immediately after the cuticle begins to appear. These observations matched well with the earlier studies (Gemne 1971), suggesting that formation of the nanostructures takes place during the pupal phase as an early and fast event preceding formation of major parts of the lens. It can be hypothesized that self-organization of the nanostructures takes place while secretions of the cone cells form the eye cuticle. As a result, near-complete nanocoatings already exist upon the lens while it is still growing (Fig. 2.6).

Summarizing the data known up to date, we can conclude that formation of the corneal nanostructures in arthropods is a complex process, which is under regulation by a series of factors. While the Turing reaction-diffusion patterning and the block copolymerisation are the two main candidates to be the underlying mechanism, we still do not possess exact information on the identity of the compounds taking part in the generation of the nanostructures, nor on the chemical nature of their interactions. On the other hand, these processes can be influenced by auxiliary mechanisms, such as dense packing bringing more order into the structures, chemical pre-patterning or topographical pre-patterning (graphoepitaxy). If it comes to the pre-patterning mechanisms, the role of the cone cell microvilli can be reconsidered, not as being an exact template upon which the nipple arrays are built, but rather as a more sophisticated tool affecting the patterning mechanisms either by chemical secretion of morphogenetically active compounds or by forming the underlying surface structure. Certain compounds secreted by the microvilli may play a role of initiating factors for nucleation of the Turing-like processes. The mesoscale structural parameters such as the lens size and shape are likely to further influence formation of the nanostructures as well. It is known that biological pat-
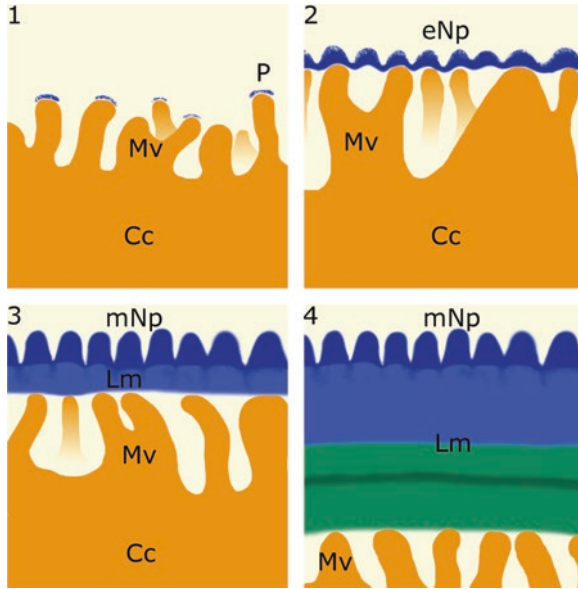
Fig. 2.6 Schematic representation of ontogenesis of the corneal nanostructures using formation of nipple arrays on the surface of a single ommatidium as an example. 1 – Secretion of the corneal material by the cone cells (Cc) with nucleation of initial patches (P) on tips of microvilli (Mv). 2 – Self-assembly of the corneal nanostructures, in this case early nipples (eNp) upon the secreting corneal material, with tips of microvilli (Mv) still attached to the inner surface of the cornea. 3 – After nanostructures are formed as mature nipples (mNp), cone cells continue to secrete the bulk lens lamina material (light blue, Lm) containing chitin and other biopolymers forming the entire lens. 4 – The lens is completely formed; lamina (light blue and green) separates the outer layer with the nanostructures from microvilli of the cone cells

terns are generated by Turing mechanism at the macro- and mesoscale (Nakamasu et al. 2009) and that artificial block copolymerization yields nanostructures with proportions an order of magnitude smaller (usually 5–10 nm in width and height) than the corneal nanocoatings of the arthropods. Thus, the arthropod corneal nanocoatings, in the matter of their size, are positioned between the traditional "zones of responsibility" of the block copolymerization and reaction-diffusion mechanisms. Although the exact chemical nature of the compounds responsible for the processes of nanopattern organization is unknown, it may be assumed that one of them could be hydrophobic – probably a wax or a lipid, while the other is of hydrophilic nature (a protein or a glycoprotein). Such a system would remind the block copolymerization outline, but also be similar to the Turing mechanism in that the hydrophobic wax or lipid would block the action of the hydrophilic protein. Investigation of the composition of the nanocoatings and of the biochemical interactions governing their formation thus remains a task of high priority in this scientific field. Actually, these questions expand the discipline of insect corneal nanostructures and touch upon the general mechanisms of biological pattern formation on the

100 nm scale. Thus, the corneal nanocoatings emerge as a remarkable model to tackle issues of general importance for biology and physics.

Finally, identification of the molecular mechanisms governing formation of the corneal nanopatterns may have technological importance. Unraveling of these mechanisms will make it possible to (bio)engineer biological or biomimetic nanostructured surfaces with desired features and parameters. Their applications for the optical, anti-wetting and self-cleaning functions discussed in this chapter may be complemented with other uses, such as the selective molecular separations, selective adsorption, or the high activity catalysis attributed to the pattern with regular sized pores resembling the dimpled pattern of the arthropod corneae (Farrell et al. 2009). Through the genetic tools provided by the model insect *Drosophila melanogaster* suitable for the study of biological nanostructures (Kryuchkov et al. 2011; Minami et al. 2016), this fruit fly can serve as a powerful instrument to further investigate the exact mechanisms of the bionanopattern formation processes, to identify the molecular interactions taking part in the generation of corneal nanocoatings, and to produce artificially designed nanopatterns with novel physical properties by means of bioengineering and synthetic biology.

References

Aghaeipour, M., Anttu, N., Nylund, G., Samuelson, L., Lehmann, S., & Pistol, M.-E. (2014). Tunable absorption resonances in the ultraviolet for InP nanowire arrays. *Optics Express, 22*(23), 29204–29212.

Anderson, M. S., & Gaimari, S. D. (2003). Raman-atomic force microscopy of the ommatidial surfaces of dipteran compound eyes. *Journal of Structural Biology, 142*(3), 364–368.

Autumn, K., Liang, Y. A., Hsieh, S. T., Zesch, W., Chan, W. P., Kenny, T. W., Fearing, R., & Full, R. J. (2000). Adhesive force of a single gecko foot-hair. *Nature, 405*(6787), 681–685.

Bernhard, C. G., & Miller, W. H. (1962). A corneal nipple pattern in insect compound eyes. *Acta Physiologica Scandinavica, 56*(3–4), 385–386.

Bernhard, C.G., Miller, W.H., & Møller, A.R. (1965). The insect corneal nipple array: A biological, broad-band impedance transformer that acts as an antireflection coating. *Zeitschrift für vergleichende Physiologie, 67*(1), 1–25.

Bhanot, P., Brink, M., Samos, C.H., Hsieh, J.C., Wang, Y., Macke, J.P., Andrew. D., Nathans, J., & Nusse, R. (1996). A new member of the frizzled family from Drosophila functions as a Wingless receptor. *Nature, 382*(6588), 225–230.

Bernhard, C. G., Gemne, G., & Sällström, J. (1970). Comparative ultrastructure of corneal surface topography in insects with aspects on phylogenesis and function. *Journal of Comparative Physiology. A, 67*(1), 1–25.

Bixler, G. D., & Bhushan, B. (2014). Rice- and butterfly-wing effect inspired self-cleaning and low drag micro/nanopatterned surfaces in water, oil, and air flow. *Nanoscale, 6*(1), 76–96.

Bixler, G. D., Theiss, A., Bhushan, B., & Lee, S. C. (2014). Anti-fouling properties of microstructured surfaces bio-inspired by rice leaves and butterfly wings. *Journal of Colloid and Interface Science, 419*, 114–133.

Blagodatski, A., Kryuchkov, M., Sergeev, A., Klimov, A. A., Shcherbakov, M. R., Enin, G. A., & Katanaev, V. L. (2014). Under- and over-water halves of Gyrinidae beetle eyes harbor different corneal nanocoatings providing adaptation to the water and air environments. *Scientific Reports, 4*, 6004.

Blagodatski, A., Sergeev, A., Kryuchkov, M., Lopatina, Y., & Katanaev, V. L. (2015). Diverse set of Turing nanopatterns coat corneae across insect lineages. *Proceedings of the National Academy of Sciences of the United States of America, 112*(34), 10750–10755.

Brongersma, M. L., Cui, Y., & Fan, S. H. (2014). Light management for photovoltaics using high-index nanostructures. *Nature Materials, 13*(5), 451–460.

Chen, H., & Chakrabarti, A. (1998). Morphology of thin block copolymer films on chemically patterned substrates. *The Journal of Chemical Physics, 108*(16), 6897–6905.

Chipman, A. D., Ferrier, D. E., Brena, C., Qu, J., Hughes, D. S., Schroder, R., Torres-Oliva, M., Znassi, N., Jiang, H., Almeida, F. C., et al. (2014). The first myriapod genome sequence reveals conservative arthropod gene content and genome organisation in the centipede *Strigamia maritima*. *PLoS Biology, 12*(11), e1002005.

Daglar, B., Khudiyev, T., Demirel, G. B., Buyukserin, F., & Bayindir, M. (2013). Soft biomimetic tapered nanostructures for large-area antireflective surfaces and SERS sensing. *Journal of Materials Chemistry C, 1*(47), 7842–7848.

Daly, H.V. (1970). The insects. Structure and function. R. F. Chapman. Elsevier, New York, 1969. *Science* 168(3935), 1082.

Deinega, A., Valuev, I., Potapkin, B., & Lozovik, Y. (2011). Minimizing light reflection from dielectric textured surfaces. *Journal of the Optical Society of America. A, 28*(5), 770–777.

Du, Q. G., Kam, C. H., Demir, H. V., Yu, H. Y., & Sun, X. W. (2011). Broadband absorption enhancement in randomly positioned silicon nanowire arrays for solar cell applications. *Optics Letters, 36*(10), 1884–1886.

Farrell, A. R., Fitzgerald, G. T., Borah, D., Holmes, D. J., & Morris, A. M. (2009). Chemical interactions and their role in the microphase separation of block copolymer thin films. *International Journal of Molecular Sciences, 10*(9), 3671–3712.

Fasolka, M. J., Harris, D. J., Mayes, A. M., Yoon, M., & Mochrie, S. G. J. (1997). Observed substrate topography-mediated lateral patterning of diblock copolymer films. *Physical Review Letters, 79*(16), 3018–3021.

Feng, L., Zhang, Y., Xi, J., Zhu, Y., Wang, N., Xia, F., & Jiang, L. (2008). Petal effect: A superhydrophobic state with high adhesive force. *Langmuir, 24*(8), 4114–4119.

Fröhlich, A. (2001). A scanning electron-microscopic study of apical contacts in the eye during postembryonic development of *Drosophila melanogaster*. *Cell and Tissue Research, 303*(1), 117–128.

Gao, X., Yan, X., Yao, X., Xu, L., Zhang, K., Zhang, J., Yang, B., & Jiang, L. (2007). The dry-style antifogging properties of mosquito compound eyes and artificial analogues prepared by soft lithography. *Advanced Materials, 19*(17), 2213–2217.

Gemne, G. (1966). Ultrastructural ontogenesis of cornea and corneal nipples in compound eye of insects. *Acta Physiologica Scandinavica, 66*(4), 511–512.

Gemne, G. (1971). Ontogenesis of corneal surface ultrastructure in nocturnal Lepidoptera. *Philosophical Transactions of the Royal Society B, 262*(843), 343–363.

Gorb, S., & Speck, T. (2017). Biological and biomimetic materials and surfaces. *Beilstein Journal of Nanotechnology, 8*, 403–407.

Green, D. W., Watson, G. S., Watson, J., & Abraham, S. J. K. (2012). New biomimetic directions in regenerative ophthalmology. *Advance Healthcare Maternité, 1*(2), 140–148.

Hamley, I. W. (1998). *The physics of block copolymers*. Oxford: Oxford University Press.

Hamley, I. W., Connell, S. D., Collins, S., Fundin, J., & Yang, Z. (2004). In situ AFM imaging of block copolymer micelles adsorbed on a solid substrate. *Abstracts of Papers of the American Chemical Society, 227*, 551–551.

Han, L., & Zhao, H. P. (2014). Surface antireflection properties of GaN nanostructures with various effective refractive index profiles. *Optics Express, 22*(26), 31907–31916.

Hancock, M. J., Sekeroglu, K., & Demirel, M. C. (2012). Bioinspired directional surfaces for adhesion, wetting, and transport. *Advanced Functional Materials, 22*(11), 2223–2234.

Helbig, R., Nickerl, J., Neinhuis, C., & Werner, C. (2011). Smart skin patterns protect springtails. *PLoS One, 6*(9), e25105.

Hensel, R., Neinhuis, C., & Werner, C. (2016). The springtail cuticle as a blueprint for omniphobic surfaces. *Chemical Society Reviews, 45*(2), 323–341.

Ivanova, E. P., Hasan, J., Webb, H. K., Truong, V. K., Watson, G. S., Watson, J. A., Baulin, V. A., Pogodin, S., Wang, J. Y., Tobin, M. J., et al. (2012). Natural bactericidal surfaces: Mechanical rupture of *Pseudomonas aeruginosa* cells by cicada wings. *Small, 8*(16), 2489–2494.

Ji, S., Park, J., & Lim, H. (2012). Improved antireflection properties of moth eye mimicking nanopillars on transparent glass: Flat antireflection and color tuning. *Nanoscale, 4*(15), 4603–4610.

Katanaev, V. L., & Kryuchkov, M. V. (2011). The eye of *Drosophil*a as a model system for studying intracellular signaling in ontogenesis and pathogenesis. *Biochemistry (Moscow), 76*(13), 1556–1581.

Kim, S. O., Solak, H. H., Stoykovich, M. P., Ferrier, N. J., de Pablo, J. J., & Nealey, P. F. (2003). Epitaxial self-assembly of block copolymers on lithographically defined nanopatterned substrates. *Nature, 424*(6947), 411–414.

Kondo, S., & Miura, T. (2010). Reaction-diffusion model as a framework for understanding biological pattern formation. *Science, 329*(5999), 1616–1620.

Kryuchkov, M., Katanaev, V. L., Enin, G. A., Sergeev, A., Timchenko, A. A., & Serdyuk, I. N. (2011). Analysis of micro- and nano-structures of the corneal surface of *Drosophila* and its mutants by atomic force microscopy and optical diffraction. *PLoS One, 6*(7), e22237.

Kryuchkov, M., Lehmann, J., Schaab, J., Cherepanov, V., Blagodatski, A., Fiebig, M., & Katanaev, V. L. (2017a). Alternative moth-eye nanostructures: Antireflective properties and composition of dimpled corneal nanocoatings in silk-moth ancestors. *J. NanoBiotechnology, 15*(1), 61.

Kryuchkov, M., Lehmann, J., Schaab, J., Fiebig, M., & Katanaev, V. L. (2017b). Antireflective nanocoatings for UV-sensation: The case of predatory owlfly insects. *Journal of Nanobiotechnology, 15*(1), 52.

Lavanya Devi, A. L., Nongthomba, U., & Bobji, M. S. (2016). Quantitative characterization of adhesion and stiffness of corneal lens of *Drosophila melanogaster* using atomic force microscopy. *Journal of the Mechanical Behavior of Biomedical Materials, 53*, 161–173.

Lee, K. C., & Erb, U. (2013). Grain boundaries and coincidence site lattices in the corneal nanonipple structure of the mourning cloak butterfly. *Beilstein Journal of Nanotechnology, 4*, 292–299.

Lee, K. C., & Erb, U. (2015). Remarkable crystal and defect structures in butterfly eye nano-nipple arrays. *Arthropod Structure & Development, 44*(6), 587–594.

Lee, K. C., Yu, Q., & Erb, U. (2016). Mesostructure of ordered corneal nano-nipple arrays: The role of 5–7 coordination defects. *Scientific Reports, 6*, 28342.

Leem, J. W., Yeh, Y., & Yu, J. S. (2012). Enhanced transmittance and hydrophilicity of nanostructured glass substrates with antireflective properties using disordered gold nanopatterns. *Optics Express, 20*(4), 4056–4066.

Lin, C., Martínez, L. J., & Povinelli, M. L. (2013). Experimental broadband absorption enhancement in silicon nanohole structures with optimized complex unit cells. *Optics Express, 21*(S5), A872–A882.

Lin, D., Fan, P., Hasman, E., & Brongersma, M. L. (2014). Dielectric gradient metasurface optical elements. *Science, 345*(6194), 298.

Liu, T. L., & Kim, C. J. (2014). Repellent surfaces. Turning a surface superrepellent even to completely wetting liquids. *Science, 346*(6213), 1096–1100.

Liu, H., Xu, J., Li, Y., & Li, Y. (2010). Aggregate nanostructures of organic molecular materials. *Accounts of Chemical Research, 43*(12), 1496–1508.

Martins, E. R., Li, J., Liu, Y., Depauw, V., Chen, Z., Zhou, J., & Krauss, T. F. (2013). Deterministic quasi-random nanostructures for photon control. *Nature Communications, 4*, 2665.

Meyer-Rochow, V. B. (1978). Retina and dioptric apparatus of the dung beetle *Euoniticellus africanus*. *Journal of Insect Physiology, 24*(2), 165–179.

Meyer-Rochow, V. B., & Stringer, I. A. N. (1993). A system of regular ridges instead of nipples on a compound eye that has to operate near the diffraction limit. *Vision Research, 33*(18), 2645–2647.

Miller, W. H. (1979). Ocular optical filtering. In H. Autrum (Ed.), *Handbook of sensory physiology* (Vol. VII/6A, pp. 69–143). Berlin/Heidelberg/New York: Springer.

Minami, R., Sato, C., Yamahama, Y., Kubo, H., Hariyama, T., & Kimura, K.-i. (2016). An RNAi screen for genes involved in nanoscale protrusion formation on corneal lens in *Drosophila melanogaster*. *Zoological Science, 33*(6), 583–591.

Mishra, M., & Meyer-Rochow, V. B. (2006). Eye ultrastructure in the pollen-feeding beetle, *Xanthochroa luteipennis* (Coleoptera: Cucujiformia: Oedemeridae). *Journal of Electron Microscopy, 55*(6), 289–300.

Miura, T., & Maini, P. K. (2004). Periodic pattern formation in reaction−diffusion systems: An introduction for numerical simulation. *Anatomical Science International, 79*(3), 112–123.

Nakamasu, A., Takahashi, G., Kanbe, A., & Kondo, S. (2009). Interactions between zebrafish pigment cells responsible for the generation of Turing patterns. *Proceedings of the National Academy of Sciences of the United States of America, 106*(21), 8429–8434.

Nickerl, J., Tsurkan, M., Hensel, R., Neinhuis, C., & Werner, C. (2014). The multi-layered protective cuticle of Collembola: A chemical analysis. *Journal of The Royal Society Interface, 11*(99), 20140619.

Oskooi, A., Favuzzi, P. A., Tanaka, Y., Shigeta, H., Kawakami, Y., & Noda, S. (2012). Partially disordered photonic-crystal thin films for enhanced and robust photovoltaics. *Applied Physics Letters, 100*(18), 181110.

Peisker, H., & Gorb, S. N. (2010). Always on the bright side of life: Anti-adhesive properties of insect ommatidia grating. *The Journal of Experimental Biology, 213*(20), 3457–3462.

Pogodin, S., Hasan, J., Baulin, V. A., Webb, H. K., Truong, V. K., Phong Nguyen, T. H., Boshkovikj, V., Fluke, C. J., Watson, G. S., Watson, J. A., et al. (2013). Biophysical model of bacterial cell interactions with nanopatterned cicada wing surfaces. *Biophysical Journal, 104*(4), 835–840.

Pratesi, F., Burresi, M., Riboli, F., Vynck, K., & Wiersma, D. S. (2013). Disordered photonic structures for light harvesting in solar cells. *Optics Express, 21*(S3), A460–A468.

Raspopovic, J., Marcon, L., Russo, L., & Sharpe, J. (2014). Digit patterning is controlled by a bmp-Sox9-Wnt Turing network modulated by morphogen gradients. *Science, 345*(6196), 566–570.

Raut, H. K., Ganesh, V. A., Nair, A. S., & Ramakrishna, S. (2011). Anti-reflective coatings: A critical, in-depth review. *Energy Environmental Sciences, 4*(10), 3779–3804.

Schuster, C. S., Morawiec, S., Mendes, M. J., Patrini, M., Martins, E. R., Lewis, L., Crupi, I., & Krauss, T. F. (2015). Plasmonic and diffractive nanostructures for light trapping−an experimental comparison. *Optica, 2*(3), 194–200.

Sergeev, A., Timchenko, A. A., Kryuchkov, M., Blagodatski, A., Enin, G. A., & Katanaev, V. L. (2015). Origin of order in bionanostructures. *RSC Advances, 5*(78), 63521–63527.

Sick, S., Reinker, S., Timmer, J., & Schlake, T. (2006). WNT and DKK determine hair follicle spacing through a reaction-diffusion mechanism. *Science, 314*(5804), 1447–1450.

Siddique, R. H., Gomard, G., & Holscher, H. (2015). The role of random nanostructures for the omnidirectional anti-reflection properties of the glasswing butterfly. *Nature Communications, 6*, 6909.

Son, J., Verma, L. K., Danner, A. J., Bhatia, C. S., & Yang, H. (2011). Enhancement of optical transmission with random nanohole structures. *Optics Express, 19*(S1), A35–A40.

Stavenga, D. G. (2006). Invertebrate superposition eyes-structures that behave like metamaterial with negative refractive index. *Journal of the European Optical Society-Rapid Publications, 1*, 06010.

Stavenga, D. G., Foletti, S., Palasantzas, G., & Arikawa, K. (2006). Light on the moth-eye corneal nipple array of butterflies. *Proceedings of the Royal Society B, 273*(1587), 661–667.

Stavroulakis, P. I., Boden, S. A., Johnson, T., & Bagnall, D. M. (2013). Suppression of backscattered diffraction from sub-wavelength 'moth-eye' arrays. *Optics Express, 21*(1), 1–11.

Sun, T. L., Feng, L., Gao, X. F., & Jiang, L. (2005). Bioinspired surfaces with special wettability. *Accounts of Chemical Research, 38*(8), 644–652.

Sun, M., Liang, A., Watson, G. S., Watson, J. A., Zheng, Y., Ju, J., & Jiang, L. (2012). Influence of cuticle nanostructuring on the wetting behaviour/states on cicada wings. *PLoS One, 7*(4), e35056.

Tanaka, G., Parker, A. R., Siveter, D. J., Maeda, H., & Furutani, M. (2009). An exceptionally well-preserved Eocene dolichopodid fly eye: Function and evolutionary significance. *Proceedings of the Royal Society B, 276*(1659), 1015–1019.

Toh, Y., & Okamura, J.-y. (2007). Morphological and optical properties of the corneal lens and retinal structure in the posterior large stemma of the tiger beetle larva. *Vision Research, 47*(13), 1756–1768.

Turing, A. M. (1952). The chemical basis of morphogenesis. *Philosophical Transactions of the Royal Society B, 237*(641), 37–72.

van Lare, M. C., & Polman, A. (2015). Optimized scattering power spectral density of photovoltaic light-trapping patterns. *ACS Photonics, 2*(7), 822–831.

Varela, F. G., & Wiitanen, W. (1970). The optics of the compound eye of the honeybee (*Apis mellifera*). *The Journal of General Physiology, 55*(3), 336–358.

Vigneron, J. P., Rassart, M., Vertesy, Z., Kertesz, K., Sarrazin, M. L., Biro, L. P., Ertz, D., & Lousse, V. (2005). Optical structure and function of the white filamentary hair covering the edelweiss bracts. *Physical Review E, 71*(1), 011906.

Watson, G. S., Watson, J. A., & Cribb, B. W. (2017). Diversity of cuticular micro- and nano-structures on insects: Properties, functions, and potential applications. *Annual Review of Entomology, 62*(1), 185–205.

Wiersma, D. S. (2013). Disordered photonics. *Nature Photonics, 7*(3), 188–196.

Wilson, S. J., & Hutley, M. C. (1982). The optical properties of 'moth eye' antireflection surfaces. *Optica Acta, 29*(7), 993–1009.

Wisdom, K. M., Watson, J. A., Qu, X., Liu, F., Watson, G. S., & Chen, C.-H. (2013). Self-cleaning of superhydrophobic surfaces by self-propelled jumping condensate. *Proceedings of the National Academy of Sciences of the United States of America, 110*(20), 7992–7997.

Wood, L. (2017). *Global nano coating market (2016–2022): Increasing technological advancement is a key driver ─ research and markets*. http://www.researchandmarkets.com/research/sqcx6v/global_nano

Wu, W., Huang, J. Y., Jia, S. J., Kowalewski, T., Matyjaszewski, K., Pakula, T., Gitsas, A., & Floudas, G. (2005). Self-assembly of pODMA-b-ptBA-b-pODMA triblock copolymers in bulk and on surfaces. A quantitative SAXS/AFM comparison. *Langmuir, 21*(21), 9721–9727.

Xiao, S. G., Yang, X. M., Edwards, E. W., La, Y. H., & Nealey, P. F. (2005). Graphoepitaxy of cylinder-forming block copolymers for use as templates to pattern magnetic metal dot arrays. *Nanotechnology, 16*(7), 324–329.

Xin, Y., Jin, H., Feng, G., Hongjie, L., Laixi, S., Lianghong, Y., Xiaodong, J., Weidong, W., & Wanguo, Z. (2016). High power laser antireflection subwavelength grating on fused silica by colloidal lithography. *Journal of Physics D: Applied Physics, 49*(26), 265104.

Xue, F., Liu, J., Guo, L., Zhang, L., & Li, Q. (2015). Theoretical study on the bactericidal nature of nanopatterned surfaces. *Journal of Theoretical Biology, 385*, 1–7.

Yoon, J. W., Lee, K. J., & Magnusson, R. (2015). Ultra-sparse dielectric nanowire grids as wide-band reflectors and polarizers. *Optics Express, 23*(22), 28849–28856.

Yu, Y. F., Zhu, A. Y., Paniagua-Domínguez, R., Fu, Y. H., Luk'yanchuk, B., & Kuznetsov, A. I. (2015). High-transmission dielectric metasurface with 2p phase control at visible wavelengths. *Laser & Photonics Reviews, 9*(4), 412–418.

Zhou, L., Dong, X., Zhou, Y., Su, W., Chen, X., Zhu, Y., & Shen, S. (2015). Multiscale micro–nano nested structures: Engineered surface morphology for efficient light escaping in organic light-emitting diodes. *ACS Applied Materials & Interfaces, 7*(48), 26989–26998.